Lab on a Chip

PAPER

View Article Online
View Journal

Cite this: DOI: 10.1039/d5lc00179j

Enhancing commercially available immunoassays through a customized electrokinetic biomolecular preconcentration device†

Barak Sabbagh, [ab] Sinwook Park[b] and Gilad Yossifon [*bc]

Immunoassays are widely utilized in various settings, from clinics and emergency rooms to remote and resource-limited environments, such as patients' homes. However, they often present a significant trade-off: while offering simplicity, speed, and cost-effectiveness, they generally lack sensitivity. This study introduces an innovative electrokinetic preconcentration device that employs ion concentration-polarization in micro- and nanofluidic systems to continuously capture and preconcentrate target biomolecules. The system then facilitates their transfer with minimal dilution to standard immunoassays, increasing analyte concentration and enhancing transport kinetics and immunoreaction rates. Designed for cost-effectiveness and ease of use, the device does not require sophisticated equipment such as pumps, making it suitable for point-of-care (POC) commercially available immunoassays. By using this device as a preliminary step for various immunoassays, including enzyme-linked immunosorbent assay (ELISA) and lateral flow assay (LFA), we achieved substantial signal enhancement, improving the limit of detection of these assays by an order of magnitude. The obtained enhancement factor correlated with processed sample volume, operational duration, and assay binding kinetics. Our experimental validations and theoretical analysis lay the groundwork for enhancing commercially available immunoassays without modifying the assays themselves, promising significant advancements in biomedical POC diagnostics.

Received 21st February 2025,
Accepted 14th July 2025

DOI: 10.1039/d5lc00179j

rsc.li/loc

Introduction

Highly sensitive biomedical assays play a crucial role in the early detection of diseases[1] and physiological conditions,[2] as well as in drug discovery,[3] and toxin detection.[4] As sensitivity increases, the assay's ability to correctly identify true-positive cases increases while the number of false-negative cases reduces. This often corresponds to a lower limit of detection (LOD) that allows for early detection and, in turn, prompt intervention and treatment, consequently resulting in a substantial enhancement in the outcomes.[5] Therefore, sensitivity and LOD are pivotal parameters for evaluating assay performance, with distinct variations observed among different diagnostic techniques.[6–8] Immunological assays (immunoassay), such as enzyme-linked immunosorbent assay (ELISA) and lateral flow assay (LFA), focus on protein detection and are considered less complex, with a trade-off of a lower sensitivity, compared to molecular biological assays as polymerase chain reaction (PCR) tests.[6] These immunoassays do not include an amplification step, as there is no equivalent to nucleic acid's PCR process for proteins. In particular, LFAs are designed for rapid and qualitative results, making them highly suitable for point-of-care (POC) testing and situations where speed, simplicity, and cost are prioritized over high sensitivity.[6,7] For comparison, the assay's LOD reaches an outstanding average level of attomolar (10^{-18} mol L^{-1}) for PCR and progressively reduces to picomolar (10^{-12} mol L^{-1}) and micromolar (10^{-6} mol L^{-1}) for ELISA and LFA, respectively.[8] Accordingly, the average cost of LFA is significantly lower than PCR and can be as low as $1 per test.[8] Therefore, there is an urgent need to enhance immunoassays to match the LOD level of molecular biological assays, while retaining their current advantages of simplicity, cost-effectiveness, and rapidity. This necessity was strongly emphasized during the recent outbreak of the COVID-19 pandemic, where LFAs were extensively used worldwide despite their frequent occurrence of false-negative results.[5] Over the years, tremendous efforts have been invested in various methodologies aimed at improving immunoassays' LOD (and sensitivity, accordingly).[6,8–11] A major focus has been placed on improving immunoreaction efficiency[14–19] or introducing signal amplification strategies applied after the immunoreaction has occurred (*e.g.*, through the use of enhanced reporters, catalytic reactions, electrochemical

[a] *Faculty of Mechanical Engineering, Technion–Israel Institute of Technology, Haifa 3200003, Israel*
[b] *School of Mechanical Engineering, Tel-Aviv University, Tel Aviv 69978, Israel. E-mail: gyossifon@tauex.tau.ac.il*
[c] *School of Biomedical Engineering, Tel-Aviv University, Tel Aviv 69978, Israel*
† Electronic supplementary information (ESI) available. See DOI: https://doi.org/10.1039/d5lc00179j

amplification, and sophisticated digital readers[12–17]). Examining each approach individually has shown a consistent 2–10-fold improvement in the LOD, reaching a point where further enhancement is difficult due to the low concentration of the target analyte. Uniquely in LFAs and microfluidic chips, the inherent flow conditions enable, in principal, the concentration of target analytes above the test region by combining convective and electro-migrative forces. However, although these electrokinetic molecular preconcentration approaches have demonstrated improvements in the LOD,[18–20] they require critical modifications to existing immunoassay platforms (*e.g.* adjustments of the buffer ionic strength and pH to enable effective electrokinetic preconcentration) and therefore not yet compatible with commercially available immunoassays. As an alternative strategy, a more universal methodology involves enriching the sample prior to its introduction into the immunoassay. Immunoassays are typically limited in the sample volume they can process, usually handling only a few microliters before mixing with buffer. As a result, in larger biological samples (*e.g.*, urine, serum, and saliva), only a small fraction is used for testing due to the assay's limited volume capacity, thereby leaving a significant portion of the sample, along with the target analytes, unused. Thus, external preprocessing of the sample by preconcentrating analytes from a large volume into a smaller assay-specific volume can enhance the assay in two ways. First, it increases the total number of analyte molecules available for immunotesting. Second, it raises the analyte concentration, improving transport kinetics and accelerating the immunoreaction rate. Methods such as magnetic beads,[21] ultrafiltration,[22] evaporation,[23] and temperature focusing[24] have been used to preconcentrate analytes in an external tube. However, these methods often require additional reagents, steps, or conditions, such as high-temperature gradients, that can be challenging or expensive to implement. Recent promising approaches use electrokinetic field-gradient focusing, based on ion concentration-polarization (ICP), to preconcentrate target analytes in an external microfluidic device prior to their introduction into the immunoassay.[25] While this technique has been extensively investigated over the years for electrokinetic preconcentration of charged molecules in aqueous electrolyte solutions within microfluidic devices,[26–29] critical challenges remain in fully realizing its potential,[30] particularly when interfacing with external assays. Several studies have begun to address these challenges. These include introducing microchannel arrays or bead bed to increase throughput and preconcentration stability,[20,31,32] continuous extraction of preconcentrated analytes,[33] multistep downstream preconcentration strategies,[34] sophisticated flow control systems with pumps for localized extraction of the preconcentrated sample,[35] and paper-based or radial microfluidic designs for processing finite sample volumes following sample extraction.[25,36] However, these improvements often come at the cost of at least one factor, for example, the inability to externally access the preconcentrated analyte plug, limited compatibility with diverse assay formats, increased system complexity requiring multiple-step operation or external equipment such as pumps, limitations in processing time or volume, or unwanted byproducts from Faradaic reactions in the preconcentrated sample. A table comparing all the mentioned methodologies, their corresponding published works, and the achieved preconcentration factors is provided in the ESI† (Table S1).

This work presents an innovative universal electrokinetic preconcentration device capable of accessible extraction a preconcentrated microliter-sized sample droplet containing target analytes, such as IgG proteins, for use in various commercial immunoassays while addressing each of the above challenges. The preconcentration mechanism used is based on ICP within microfluidic channel array with continuous fluid flow, enabling extensive sample processing over time without any physical restriction on the introduced sample volume. This allows for a dramatic increase in the number of trapped analytes over time, and correspondingly, their concentration due to volume reduction. By utilizing the built-in hydraulic pressures within the microfluidic device, the preconcentrated target analytes can be effectively transferred to a collection chamber with an accessible opening to the open air, eliminating the need for external pumps and minimizing the collection of unwanted electrochemical byproducts generated at the electrodes. From there, the analytes can be directly introduced as microliter-sized sample droplets into the immunoassay, without the need for elution, ensuring compatibility with a wide range of assays. Applying these principles has allowed us to present a significant improvement of up to one order of magnitude in the sensing capabilities of various IgG antibodies in both ELISA and LFA kits using the same universal preconcentration device. This simplifies and generalizes the integration between the preconcentration device and the chosen immunoassay, while enhancing the immunoassay's limit of detection and sensitivity as a function of the preconcentration factor.

Results and discussion

Working principle of the external electrokinetic preconcentration device

A schematic illustration of the preconcentration device and the preconcentration process prior to the immunoassay testing is shown in Fig. 1. The device was designed for continuous ICP-based preconcentration within the main microfluidic channel, followed by advective transfer with minimal dilution of the preconcentrated analytes to a collection chamber. The collection chamber was connected to the main channel *via* two side channels and featured an opening in its top substrate (Fig. 1a–c). This opening served as a fluid outlet, allowing direct sample extraction without passing through the electrode reservoirs, which may contain byproducts from electrochemical reactions. Additionally, the opening acted as a valve to regulate flow through the side channels. By initially sealing the opening, we suppressed any

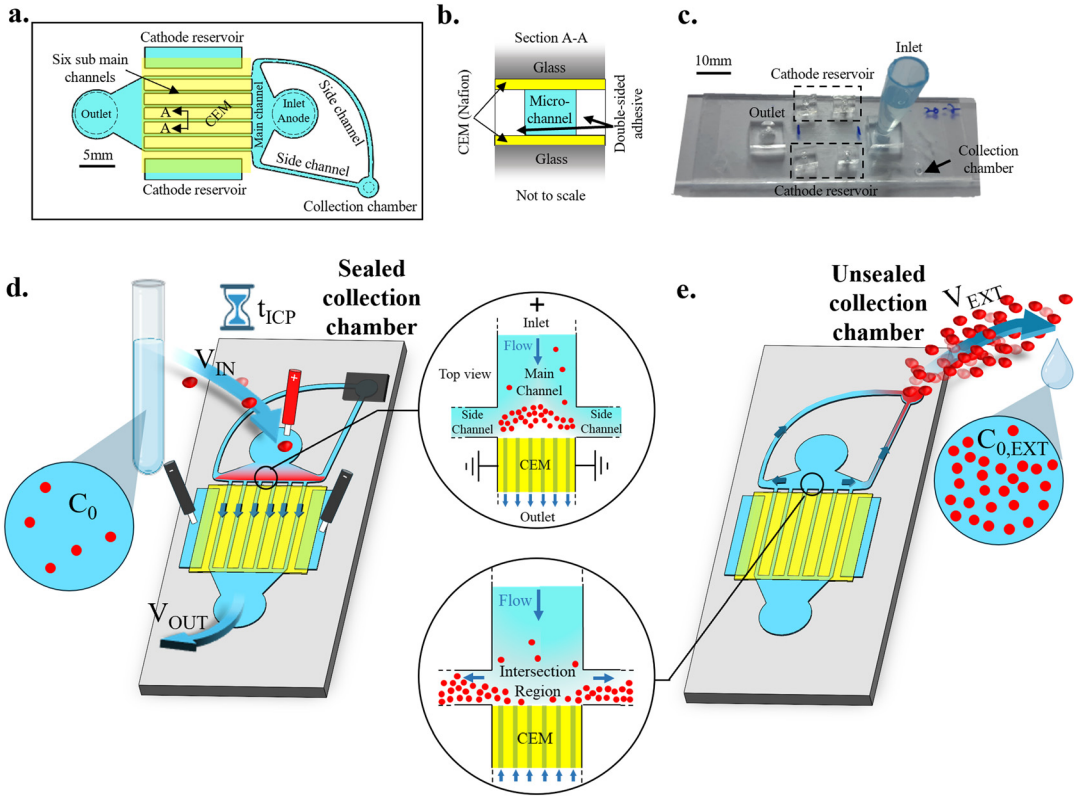

Fig. 1 Schematic representation of the working principle of the external preconcentration device. a. Top view of the chip design, where turquoise, yellow, and white colors represent the microfluidic channels (main and side channels), the cation exchange membrane (CEM), and the double-sided adhesive, respectively. b. Side view of the A–A cross section of one of the sub-main channels at the device's center. c. A picture of the device. d. and e. Working principle: d. a large sample volume (V_{IN}) with analyte concentration C_0 is introduced into the device's inlet reservoir, while the collection chamber remains sealed. Applying an electrical current across the CEM induces ionic concentration–polarization (ICP), preconcentrating negatively charged analytes at the intersection of the main microfluidic channel with the CEM. e. When desired, the accumulated analytes are advectively transferred through the side channels into the collection chamber by unsealing it. Extracting the solution from the collection chamber (with volume $V_{EXT} \ll V_{IN}$) results in an increased analyte concentration $C_{0,EXT}$, amplified by a factor of [P], which is proportional to V_{OUT}/V_{EXT} (where V_{OUT} is the processed solution volume reaching the outlet reservoir).

driving force that could induce advective flow toward the collection chamber. As a result, the introduction of a fluid sample (with volume V_{IN}) into the device's inlet reservoir generated a pressure-driven flow exclusively through the main channel, connecting the inlet and outlet reservoirs. Through the utilization of fluidic platforms consisting of micro-sized structures (*i.e.*, microchannels) interfacing with nano-sized structures (*i.e.*, a cation exchange membrane, CEM), ICP is generated upon the application of an electric potential difference $\Delta\phi$.[37,38] This spatial polarization in ion concentration sets up an intensified electric field at the ion depletion layer, which, in turn, increases the electrostatic forces and corresponding electrophoretic velocity of charged analyte molecules. Balancing the electrophoretic velocity with counteracting advection allows for reaching a local equilibrium, where a continuous trapping of charged analytes becomes possible. Therefore, by simultaneously combining ICP with counteracting pressure-driven and electro-osmotic fluid flow, anionic analytes, *e.g.*, proteins in alkaline conditions (pH $>$ 7),[39] were preconcentrated over time t_{ICP} (Fig. 1d). When desired, the preconcentrated analytes were advectively transferred to the collection chamber by simply punching its seal (Fig. 1e). A thin adhesive tape was used to seal the chamber (see Method section for details), allowing holes to be punched without excessive force or debris formation, thereby preventing backflow and blockage of the microchannel. Reopening the seal and exposing the collection chamber to atmospheric pressure induced an additional flow driven by the hydraulic pressure difference between the intersection region of the side channels and the collection chamber. The device was designed so that the ICP-based preconcentration occurs near this intersection region, facilitating the effective transfer of the accumulated analytes, as experimentally demonstrated in the following sections (Movie S1†).

The preconcentration ratio ([P]) between the concentration of the target analyte in the extracted sample from the collection chamber ($C_{0,EXT}$) and the concentration of the initial sample (C_0) is proportional to the volume ratio V_{OUT}/V_{EXT}, where V_{OUT} is the processed volume through the main channel (*i.e.*, the volume in the outlet reservoir) and V_{EXT} is the volume of the extracted sample. As the

accumulation and the transfer efficiencies approach ideality (*i.e.*, all analyte molecules are trapped and transferred to the collection chamber), the resulting [P] will converge toward this volume ratio. Therefore, as more fluid is processed through the main channel (*i.e.*, increased V_{OUT}) and less fluid is extracted from the collection chamber (*i.e.*, decreased V_{EXT}), a higher [P] is expected. While V_{EXT} should not be reduced below the minimum sample volume required for testing in the immunoassay, V_{OUT} can be continuously increased, along with [P], until reaching the maximal capacity for molecule accumulation, where the exact value warrants separate investigation beyond the current study.

Experimental characterization of the device

The flow field, ICP-based preconcentration of a target analyte, and the advective transfer of the preconcentrated analyte to

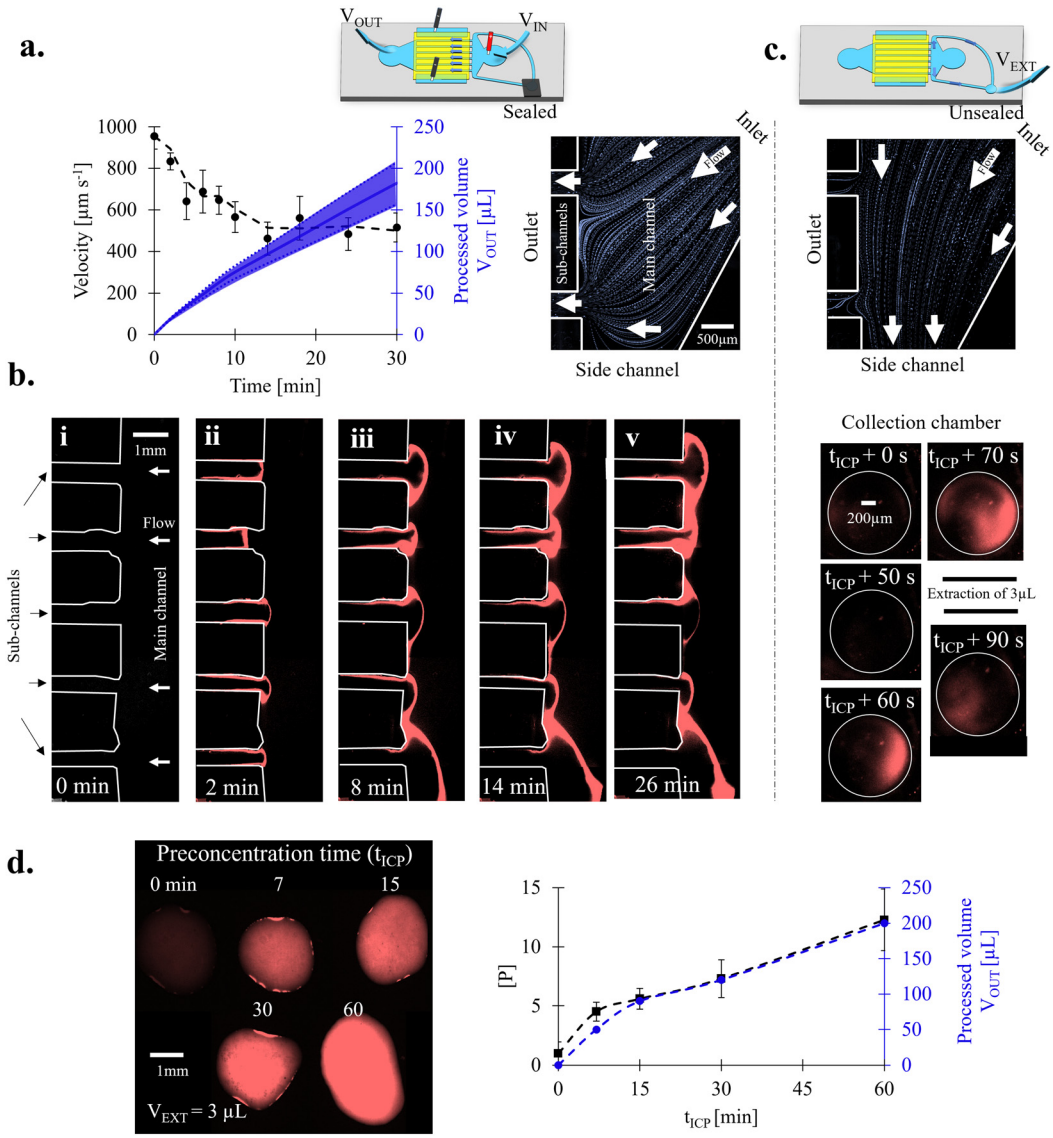

Fig. 2 Experimental characterization of the ICP-based preconcentration and corresponding enhancement factor [P]. a. Left: Measured flow velocity (●) and estimated processed volume (—, V_{OUT}) over time under the conditions of a sealed collection chamber, V_{IN} = 500 μL, and $\Delta\phi$ = 200 V. Right: Particle trajectory plot showing directional flow from the inlet to the outlet reservoirs through two sub-main channels, with no flow observed towards the side channel. b. Visualization of the intersection region between the sub-channels and the main channel over time (from left to right ((i)–(v)): 0, 2, 8, 14, 26 minutes) during the ICP-based preconcentration of fluorescent analyte molecules (DyLight® 488, colored in red). c. Top: Particle trajectory plot immediately after unsealing the collection chamber and turning off the electric field ($\Delta\phi$ = 0), showing flow directed towards the side channel. Bottom: Visualization of the collection chamber from the moment it is unsealed (t_{ICP} + 0 s) until the majority of the preconcentrated analyte is transferred to the collecting chamber (at t_{ICP} + 70 s), followed by manual extraction of 3 μL (at t_{ICP} + 90 s). d. The analyte concentration enhancement factor [P] as a function of t_{ICP} (and the corresponding processed volume V_{OUT}). [P] (■) was evaluated by comparing the measured fluorescence intensities to the initial intensity, while V_{OUT} (●) was determined by extracting at t_{ICP} and measuring the solution volume from the outlet reservoir, thus verifying the volume estimation in section a.

the collection chamber were visualized under a microscope to characterize the device operation (Fig. 2). As shown in Fig. 2a, when the collection chamber was sealed and a sample was introduced into the inlet reservoir while applying an electric field, a combined electro-osmotic and pressure-driven flow occurred from the inlet to the outlet reservoir. A gradual decrease over time in flow velocity (and correspondingly flow rate) was observed due to the continuous transport of liquid between the two reservoirs, which reduced the hydrostatic pressure difference. In the current configuration, introducing 500 μL (= V_{IN} at t = 0 min) to the inlet reservoir resulted in an initial flow rate of 955 ± 61 μm s^{-1}, which gradually decreased to 514 ± 69 μm s^{-1} after 30 minutes of operation. This setup allowed for the processing of approximately 180 ± 25 μL (= V_{OUT} at t = 30 min) of the sample during this period, achieving stability and high effectiveness in the ICP-based preconcentration with an average flow rate of 6 ± 1 μL min^{-1} (Fig. 2b).

Using negatively charged fluorescent molecules as the target analyte, we confirmed their preconcentration at the intersection region of the main and side channels by measuring the emitted light intensity (Fig. 2b). We observed a gradual increase in both intensity and width of the preconcentration plug over time as more sample was processed, resulting in the continuous accumulation of additional molecules. To stabilize the ICP and minimize vortex induction,[40] which could reduce trapping effectiveness,[31] the main channel split into six narrower sub-channels downstream of the intersection region.

Unsealing the collection chamber resulted in the advective transfer of liquid from the intersection region to the collection chamber (Fig. 2c) (Fig. S7†). The observed flow field from both the inlet and outlet reservoirs toward the side channels ensured effective transfer of accumulated analyte, regardless of their exact location (Movie S2†). The increased fluorescence intensity in the collection chamber indicated that, after 30 minutes of processing, the preconcentrated analyte was successfully transferred within 70 seconds upon seal removal (Fig. 2c). Accordingly, the fluorescence intensity at the intersection region decreased to its initial value (at t = 0 min), indicating no absorption of the analyte to the channel's surfaces. A subsequent extraction of 3 μL (= V_{EXT}) from the collection chamber returned the fluorescence intensity within the chamber to its initial low level as well. Comparing the fluorescence intensity of the extracted liquid of ~3 μL with that of the initial solution showed a ~10-fold increase, corresponding to an identical concentration change [P] of the target analyte (Fig. S8†). Adjusting the preconcentration time (t_{ICP}) and the corresponding extracted volume (V_{EXT}) altered [P] accordingly (Fig. 2d). Consequently, the intensity in the outlet reservoir dropped to nearly zero as majority of the fluorescent molecules were trapped upstream (Fig. S9 and S10†).

To prevent any effects from reactions occurring at the anode electrode in the inlet reservoir, such as changes in pH and gas bubble generation, the initially introduced sample volume in the inlet reservoir (V_{IN}) was set to be significantly larger than the expected V_{OUT}. This approach ensured an ample sample reservoir of at least hundreds of microliters, maintaining stable conditions throughout the operation. Consequently, eliminating the collection chamber and extracting the preconcentrated analyte directly from the inlet reservoir would dramatically reduce the obtained [P], as V_{EXT} would be constrained by the substantial fluid volume remaining in the inlet reservoir.

Theoretical evaluation of the signal enhancement

To evaluate the expected signal enhancement in various immunological assays due to preconcentration, we must investigate the kinetics of transport and binding reactions. For this end, we employed a simplified one-dimensional

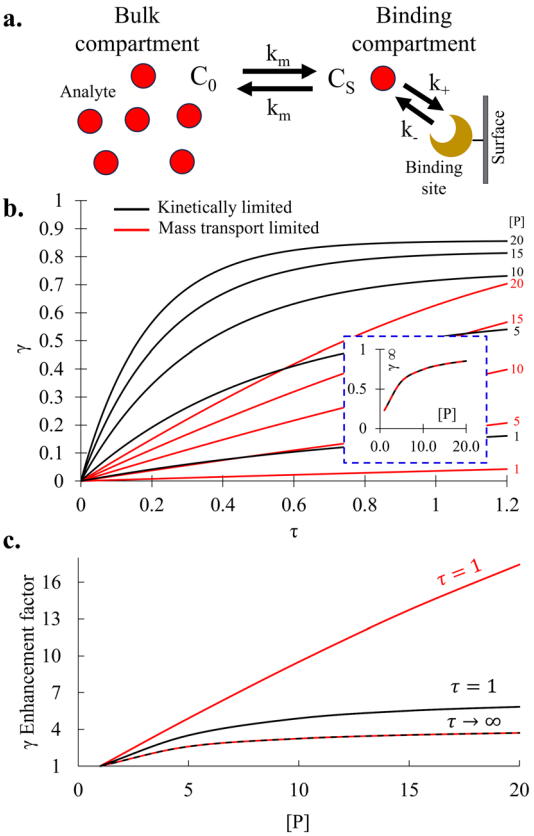

Fig. 3 Theoretical assessment of signal enhancement. a. Schematic illustration of the simplified one-dimensional model used to describe the kinetically and mass-transport-limited reversible binding of a mobile analyte (red dots) in the bulk to immobilized binding sites (yellow crescent moons) on a plane surface. C_0 and C_S represent the analyte concentrations in the bulk and near the plane surface. k_+, k_-, and k_m are the association, dissociation, and mass transport rate constants, respectively. b. Sensor's relative signal (γ) as a function of normalized time (τ) for concentration increase factor [P] = 1, 2, 4, 8, 16, 20. Black and red lines represent kinetically and mass-transport limited conditions, respectively. The inset shows the steady-state relative signal (γ^{∞}) without a time limit, where both conditions converge to the same value (dashed black and red line). c. Relative signal enhancement factor at τ = 1 and $\tau \to \infty$ for the examined [P] values (1 to 20).

model that divides the mass transport-dependent binding of mobile analyte in the bulk to immobilized probes on a planar surface into two compartments (Fig. 3a).[41] The first stage addresses the transport of an analyte from the bulk compartment to the binding compartment (*e.g.*, immobilized probes) (eqn (1)), while the second stage covers the reversible binding process (eqn (2)). Additional details about the model can be found in the Methods section and ESI.† By solving the model with increased analyte concentrations (C_0) scaled by a factor of [P], we illustrate the dynamic change in the sensor's relative signal (γ) as a result of preconcentration (Fig. 3b).

For generality, we examined two cases: mass transport-limited and kinetically limited bindings, represented by red and black lines in Fig. 3b and c, respectively. Each case correlates with different immunological assays depending on the overall conditions. The built-in flow and micro-sized pores in LFAs lead to kinetically limited binding, whereas in milli/microliter plate ELISAs, binding is typically mass-limited.[42] As depicted in Fig. 3, for both cases, increasing the analyte concentration by a factor of [P] enhances γ. For comparison, under the given parameters (detailed in the Method section) and time $\tau = 1$, γ increases from approximately 0.14 to 0.85 by gradually increasing C_0 by a

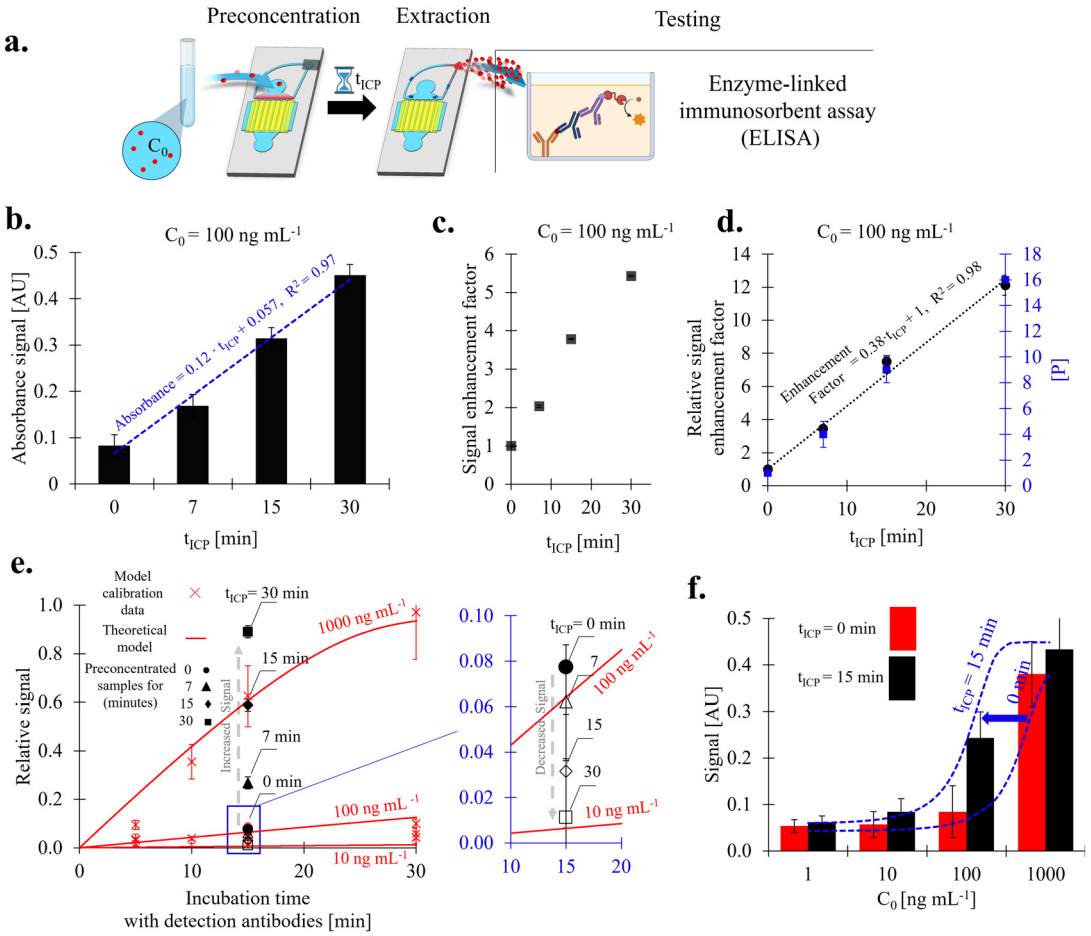

Fig. 4 Enhancing enzyme-linked immunosorbent assays (ELISAs) using the preconcentration device. a. Schematic of the testing procedure, including (from left to right) the introduction of the sample solution to the preconcentration device, preconcentration of a target analyte for t_{ICP} minutes, extraction of the preconcentrated analyte into ~3 μL sample volume, and testing in the ELISA according to its official protocol. b. Absorbance signals (in arbitrary units AU) obtained in the ELISA for C_0 = 100 ng mL^{-1} of fluorescently labeled IgG1 after preconcentration for t_{ICP} = 0, 7, 15, and 30 minutes. c. Signal enhancement factor calculated from part b. d. The relative signal enhancement factor (●) and the corresponding preconcentration factor [P] (■), as evaluated from part e. The relative signal was calculated by subtracting the noise level and normalizing with the maximum signal received for optimal IgG concentration of C_0 = 1.5 μM mL^{-1}. e. ELISA standard curves (—) obtained by fitting the mass-transfer limited model to the experimentally obtained relative signals (×) for known concentrations (10, 100, and 1000 ng mL^{-1} of IgG1) and varied incubation time with detection antibodies (0, 7, 15, 30 min). The relative signals from testing preconcentrated samples at C_0 = 100 ng mL^{-1} of IgG, with 15 minutes of incubation time and t_{ICP} values of 0 (●), 7 (▲), 15 (♦), and 30 (■) minutes, are also shown. Additionally, relative signals from samples collected from the outlet reservoir are displayed in the inset (△, ◇, □, for t_{ICP} = 7, 15, 30 min, respectively). These samples were collected simultaneously with the preconcentrated samples from the collecting chamber. A full description of the fitting parameters for the theoretical model applied to the experimental signals can be found in the ESI.† f. Absorbance signals (in AU) for non-labeled IgG3 concentrations ranging from 1 to 1000 ng mL^{-1}, measured without preconcentration (t_{ICP} = 0, red column) and with 15 minutes of preconcentration (t_{ICP} = 15 min, black column). Sigmoidal curves (– –) were fitted to the signals.

factor of [P] = 20, resulting in an enhancement factor of 5.8 in the relative signal ($\gamma_{C_0 \cdot 20}(\tau = 1)/\gamma_{C_0}(\tau = 1)$) for the kinetically limited case. The enhancement factor in the relative signal further increased to 17.4 under mass-transport limitation, owing to its roughly linear dependency on the bulk concentration for $\gamma \ll 1$.[41] Examining the steady-state relative signal, γ^{∞} shows much lower enhancement factors due to the unlimited binding time, reaching up to an enhancement factor of 3.7 for [P] = 20 for both cases (Fig. 3c). However, achieving γ^{∞} in immunological assays, particularly in mass-limited POC diagnostics, is unrealistic as results need to be provided within a limited and reasonable time. Therefore, assay time must also be considered in realistic scenarios.

Experimental signal enhancements of ELISA

A sample containing C_0 = 100 ng mL^{-1} of fluorescently labeled mouse IgG1 was preconcentrated using the device for t_{ICP} times of 7,15, and 30 minutes, extracted into 3 μL (= V_{EXT}), and tested in the ELISA according to its official testing procedure (Fig. 4a). The preconcentration and extraction of the labeled IgG were verified by visualizing the fluorescence intensity over time (Fig. S10†). Results indicated that preconcentrated samples showed enhanced signals, increasing from 0.083 AU for t_{ICP} = 0 (*i.e.*, non-preconcentrated sample) to 0.450 AU for t_{ICP} = 30 min (Fig. 4b), achieving a maximum signal enhancement factor of approximately 5.5 (Fig. 4c). Subtracting the background noise (0.048 AU) from the measurements resulted in higher enhancement factors, reaching up to ~12 (Fig. 4d). The corresponding concentration increase ratio [P] was theoretically evaluated by fitting the mass-limited reaction model to these signals after normalizing them (Fig. 4e). This analysis estimated a concentration increase by [P] = 4, 9, 16 ± 1 to $C_{0,EXT}$ = 400, 900, 1600 ± 100 ng mL^{-1} for t_{ICP} = 7, 15, and 30 min, respectively (Fig. 4d). When plotting the relative signals on the ELISA standard curves, a gradual enhancement of the obtained signals was observed, with values starting from the 100 ng mL^{-1} curve (for t_{ICP} = 0 min) surpassing those from the 1000 ng mL^{-1} curve (for t_{ICP} = 30 min). (Fig. 4e). Additionally, 3 μL samples from the outlet reservoir of the device were tested as controls and were expected to produce the lowest signal compared to the other samples due to the absence IgG. These signals fell below the 100 ng mL^{-1} curve toward the 10 ng mL^{-1} curve (Fig. 4e), reinforcing that, although the trapping efficiency was not perfect, a significant percentage of the IgG was collected in the preconcentrated sample. We also evaluated the advantage of the preconcentration step over an extended incubation time with the detection antibodies of the ELISA kit (Fig. 4e). For example, with 15 minutes of preconcentration of C_0 = 100 ng mL^{-1} followed by the standard 15 minutes of incubation with detection antibodies (totaling 30 minutes), a high relative signal of 0.588 AU was obtained. In contrast, without preconcentration (t_{ICP} = 0 min) and with 30 minutes of incubation (totaling 30 minutes), the signal was six times lower at 0.09 AU (Fig. 4e). This preference for preconcentration is attributed to the increased concentration of the analyte and the corresponding higher association rate (Fig. 3c). Furthermore, testing various non-labeled IgG3 concentrations ranging from C_0 = 1–1000 ng mL^{-1} after t_{ICP} = 15 min of preconcentration improved assay sensitivity from 3.1×10^{-4} to 1.8×10^{-3} AU per 1 ng mL^{-1} of IgG in the sensing range (Fig. 4f), resulting in a tenfold improvement in the LOD to 1 ng mL^{-1}. Without preconcentration, 1 ng mL^{-1} IgG3 was undetectable, with the signal approaching the noise level of 0.053 AU. However, after only 15 minutes of preconcentration, the signal increased to 0.061 AU, bringing it into the detectable range. At concentrations above 1000 ng mL^{-1}, preconcentration had no effect, as the signal approached its maximum value with most binding sites already occupied. Similarly, at IgG3 concentrations below 1 ng mL^{-1}, 15 minutes of preconcentration had no effect, indicating that [P] did not exceed tenfold.

Experimental signal enhancements of LFA

Replacing ELISA with LFA, while using the same universal preconcentration device and following the same overall procedure, presented a similar trend of signal enhancement (Fig. 5). However, unlike ELISA, which detects a single analyte type per well, the inherent flow in LFA allows for simultaneous detection of multiple analytes on the same testing strip. An example for such multiplexing capability is the IgG isotyping LFA, which is designed to simultaneously detect IgG1, IgG2a, IgG2b, and IgG3.

Additionally, LFAs intended for POC use are typically assessed with the naked eye and interpreted qualitatively as either positive or negative based on the visibility of the test lines. Testing various IgG concentrations ranging from 1 ng mL^{-1} to 50 μg mL^{-1} in the IgG isotyping LFA revealed a limit of detection threshold of 500 ng mL^{-1} of IgG, below which the test lines were not visible (*i.e.*, negative readout) (Fig. S3†). When a sample solution was spiked with two types of IgG, 50 ng mL^{-1} of IgG3 and 500 ng mL^{-1} of fluorescently tagged IgG1, the corresponding test lines exhibited a marked increase in visibility (*i.e.*, positive readout) after 60 minutes of preconcentration followed by the assay (Fig. 5a and b). This improved the LFA's limit of detection by at least one order of magnitude to 50 ng mL^{-1}.

A qualitative comparison of the color intensity of the test line after preconcentration, compared to that from known concentrations, estimated the concentration increase factor [P] to be between 10- and 100-fold (Fig. S3†). This estimation is consistent with the volume ratio V_{OUT}/V_{EXT} (160/3), which provides an ideal upper limit of 53 for [P]. Furthermore, testing 3 μL from the outlet reservoir after preconcentration revealed invisible lines, as expected.

Quantitative analysis of the test lines color intensity, captured through imaging, indicated a signal enhancement factor of up to 3.5-fold following preconcentration (Fig. 5c). This observed signal enhancement for both test lines validated the effective preconcentration and extraction of both IgG types during a single device operation, despite

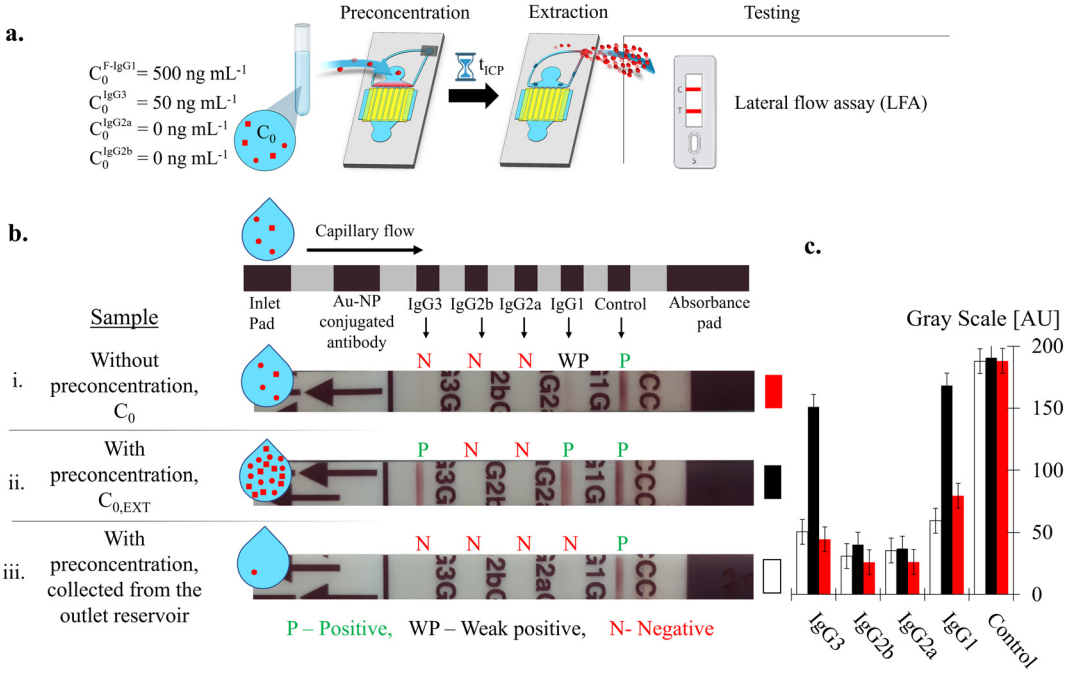

Fig. 5 Enhancing lateral flow assays (LFAs) using the external preconcentration device. a. Schematic of the testing procedure steps (similar to ELISA in Fig. 5) for a solution containing 0.5 μg mL^{-1} of fluorescent-tagged IgG1, 50 ng mL^{-1} of IgG3, and 0 ng mL^{-1} of IgG2a and IgG2b. b. Qualitative comparison of the obtained signals (*i.e.*, the intensity of the red line near the IgG3, IgG2b, IgG2a, and IgG1 testing regions) from a mouse isotyping IgG LFA by testing: i. A sample with the initial IgG concentrations C_0 (*i.e.*, without preconcentration), ii. A preconcentrated sample with increased IgG concentrations ($C_{0,EXT}$) after t_{ICP} = 60 min, iii. A sample from the outlet reservoir of the device after t_{ICP} = 60 min. All samples were collected, tested, and interpreted simultaneously. The images of the test strips represent the approach used by a home user to evaluate the assay results. c. Quantitative comparison of the obtained signals after grayscale conversion (Fig. S11†). The red, black, and white columns represent samples i., ii., and iii., respectively.

potential variations in the electromobilities of the IgGs (especially due to the fluorescent tagging of IgG1). Additionally, the test lines for IgG2b and IgG2a remained negative across all samples, confirming that the assay's specificity was unaffected by the preconcentration process.

Conclusions

In conclusion, this study demonstrated significant signal enhancement in various commercial immunological assays, including ELISA and LFA, achieved through a preliminary preconcentration step utilizing an external electrokinetic preconcentration device. The device was innovatively designed and fabricated with low-cost materials and straightforward protocols, enabled rapid and robust prototyping. The use of pressure-driven and electro-osmotic flow throughout the preconcentration and transfer process maintained the operational simplicity essential for POC diagnostics. The unique design of the microfluidic channels within the device effectively addressed major challenges commonly encountered in ICP-based preconcentration, such as stabilizing the flow and ensuring precise control over the location of the preconcentrated analytes. Microscopic visualization confirmed the device's effectiveness in preconcentrating negatively charged target molecules over time, with the ability to extract a small microliter-sized sample on demand for external use. When the preconcentrated sample was introduced into a commercially available immunoassay and tested according to its standard procedure, significant signal enhancement was observed, correlating with the achieved concentration increase ratio [P]. The longer the preconcentration device operated, the higher the obtained [P], leading to more pronounced signal enhancement in the assay and improved limits of detection. Furthermore, the benefits of investing time in performing preconcentration prior to ELISA, rather than extending the incubation time with probe antibodies during the assay itself, have been demonstrated. This clear preference for preconcentration is attributed to the increased concentration of the target analytes. These correlations were supported by a theoretical model that considered mass-limited and kinetically limited reversible bindings, emphasizing the critical role of the preconcentration device across different immunoassays. Maximizing the throughput of the preconcentration device to accommodate higher flow rates and volumes, while progressing toward full automation, would further enhance its practical application and scalability. The approach marks a significant step toward leveraging the advantages of micro- and nanofluidics to enhance commercially available immunoassays, potentially leading to more rapid, accurate diagnostic processes, improved patient diagnostic outcomes, and advancements in the point-of-care diagnostics.

Methods

Device fabrication

The fabrication method of the device and the materials used were optimized for cost-effectiveness and simplicity in immunoassays. In brief, a 25 μm thick double-sided adhesive (3M™ Optically Clear Adhesive 8146-1-ND) was cut using a Silhouette Cameo 4 and sandwiched between two clean glass slides (70 × 50 mm, Sigma) to form the microfluidic channels of the device (Fig. 2a–c). Prior to assembly, the top glass slide was drilled (Dremel 4000 with Diamond grinding bit ∅1.8 mm, Proxxon) at three designated locations for the inlet, outlet, and collection chambers. Additionally, four holes were drilled to allow for wetting and the insertion of two external cathode electrodes into the side reservoirs for voltage application. After drilling, the central surface area (15 × 18 mm) on both the top and bottom glass slides was spin-coated with 100 μL of CEM (Nafion™ perfluorinated resin solution 1100 W, Sigma) for 30 seconds at 2000 rpm. Kapton tape was used as a mask to prevent coating outside this area and was removed after heating at 50 °C for 3 hours. Reservoirs made of 1 mL tubes, which were inserted into 1 : 10 (base : cross-linker) polydimethylsiloxane (PDMS) blocks were attached with adhesive to the outer plane of the top slide. The on-demand sealing of the opening (*i.e.*, the drilled hole) in the collection chamber was achieved using a 55 μm thick adhesive tape (Magic™ Tape, Scotch©), applied directly over the opening and preventing any fluid flow. More details on the fabrication process can be found in the supporting information.

Solution preparation

A 50 mM Tris buffer (Trizma®, Sigma-Aldrich™) served as the medium (pH 10, conductivity 0.35 mS cm^{-1}), into which different proteins (mouse IgG3, IgG2b, and mouse IgG1 conjugated with Alexa Fluor® 488, AbcamTM) serve as analytes with known concentrations (0.1–1000 ng mL^{-1}) were spiked, preconcentrated, and tested using ELISA and LFA (Fig. 4 and 5). For the experimental characterization of the device, KCl buffer (pH 7, 0.4 mS cm^{-1}) spiked with 0.1 μM DyLight® 488 NHS Ester (Thermo Scientific™) was utilized (Fig. 2).

Experimental setup

To generate ICP, a voltage drop of up to $\Delta\phi$ = 200 V was applied across the device using a Potentiostat (Keithley 2636) and platinum electrodes (0.5 mm diameter, Surepure Chemetals). To achieve optimal ICP conditions, $\Delta\phi$ was gradually increased from 50 V until a stable preconcentration plug was formed and remained stable over time. The electrodes were immersed in the solution, with the anode (+) positioned in the inlet reservoir and the two cathodes (−) placed in two side reservoirs. The side reservoirs were electrically connected to the main microfluidic channel through the coated CEM, ensuring that the electrical current passed through it. The CEM's poor solvent permeability suppressed any advective flow between the side reservoirs and the main channel, which also minimized the transfer of byproducts generated at the cathode electrodes to the main channel and helped prevent significant pH alterations. A few hours prior to operation, the chip was cleaned and wetted with the working solution. For ICP-based preconcentration, the target solution was first introduced into the inlet reservoir to induce pressure-driven flow, after which $\Delta\phi$ was applied. Immediately afterward, the solution from the outlet reservoir was removed to accurately evaluate the processed volume during the operation (V_{OUT}). To collect the preconcentrated analyte (V_{EXT}), the tape covering the opening of the collection chamber was punctured with an 18G needle, and the solution was directly pipetted out. For the experimental characterization of the device (Fig. 2), the average velocity and the corresponding standard deviation at a specific time were calculated based on trajectory tracking of at least 15 particles (1 μm diameter) over 500 ms. Using the obtained temporal velocities and the channel geometry at the measurement point (25 μm height and 7 mm width), the processed volume as function of time was calculated by trapezoidal numerical integration method (MATLAB™). To visualize the device microchannels, a spinning disk confocal system (Yokogawa CSU-X1), an inverted microscope (Eclipse Ti-U, Nikon), and a camera (Andor iXon3), were used.

Assay procedures

All testing was conducted using commercially available mouse immunoglobulin G (IgG) isotyping immunoassays, as they are non-pathogenic, available in both assay types, and widely used for IgG subclass profiling.[43] Mouse isotyping ELISA (ab273149, Abcam) and LFA (ab190514, Abcam) kits were utilized according to their assay procedures as described in the ESI,† including use of the commercially available dilution buffer that comes with the test kit to maintain optimal pH and ionic strength conditions during the assay. Notably, no effect on sensing was observed for fluorescently labeled antibodies compared to non-labeled antibodies for both LFA and ELISA.

Theoretical model

The overall kinetics, under the steady-state approximation of a fully developed concentration gradient, *i.e.*, $dC_s/dt = 0$, are described by the following two coupled nonlinear differential equations

$$\frac{dS}{dt} = k_m(C_0 - C_s), \quad (1)$$

$$\frac{dS}{dt} = k_+ C_s\left(S^{MAX} - S\right) - k_- S, \quad (2)$$

where S and S^{MAX} are the current and maximum signal responses (in AU). S and S^{MAX} are proportional to the surface concentration of formed antibody/antigen complex sites and free bindings sites at t = 0, respectively. C_0 and C_s (in M) are the analyte concentrations in the bulk and at the binding

region, respectively. k_+ (M^{-1} s^{-1}), k_- (s^{-1}), and k_m (AU M^{-1} s^{-1}) are association, dissociation, and mass transport rate constants, respectively. The mathematical model was derived from previously published studies,[41,42] while a few adjustments were made to express the effect of preconcentration on the binding kinetics on S, including multiply C_0 by a factor of [P] (*i.e.*, replacing C_0 with C_0[P]). Further details are provided in the ESI.† For representation, we define the relative signal as $\gamma = S/S^{MAX}$ ($0 \le \gamma \le 1$) and the dimensionless time as $\tau = t(k_+ C_0 + k_-)$. The overall assay is considered mass-transport limited when $k_m \ll k_+ S^{MAX}$ and kinetically-limited when $k_+ \ll k_m S^{MAX}$.[41] For the theoretical assessment of signal enhancement (Fig. 3), the following parameters were used: C_0 = 0.3 nM, $k_+ = 1.0 \times 10^6$ M^{-1} s^{-1}, $k_- = 1.0 \times 10^{-3}$ s^{-1}, S^{MAX} = 1 AU. In the mass-transport limited case, k_m was set to 2.0×10^5 AU M^{-1} s^{-1}, while in the kinetically limited case, k_t was assumed to approach infinity. For fitting the experimental results (Fig. 4d, S6†), the following parameters were used: C_0 = 0.06 nM, $k_+ = 1.2 \times 10^6$ M^{-1} s^{-1}, $k_- = 3.9 \times 10^{-3}$ s^{-1}, $k_m = 1.2 \times 10^5$ AU M^{-1} s^{-1}, and S^{MAX} = 1 AU.[44]

Data availability

The authors confirm that the data supporting the findings of this study are available within the article and as its ESI.†

Author contributions

B. S., S. P., and G. Y. conceived the research idea and developed the study design. B. S. fabricated the devices, conducted the experiments, analyzed the data, and developed the analytical model. S. P. and G. Y. contributed to interpreting the results. G. Y. supervised the planning of the study and the writing of the manuscript. All authors contributed to writing and reviewing the manuscript.

Conflicts of interest

A patent application related to the findings reported in this manuscript has been filed by G. Y., B. S. and S. P.

Acknowledgements

We acknowledge the financial support of the Ministry of Innovation, Science & Technology (MOST), Israel [grant #4768].

References

1 J. Wu, Z. Fu, F. Yan and H. Ju, Biomedical and clinical applications of immunoassays and immunosensors for tumor markers, *TrAC, Trends Anal. Chem.*, 2007, **26**(7), 679–688.
2 J. Kim, A. S. Campbell, B. E. F. de Ávila and J. Wang, Wearable biosensors for healthcare monitoring, *Nat. Biotechnol.*, 2019, **37**, 389–406.
3 D. Yu, B. Blankert, J. C. Viré and J. M. Kauffmann, Biosensors in drug discovery and drug analysis, *Anal. Lett.*, 2005, **38**, 1687–1701.
4 P. Nolan, S. Auer, A. Spehar, C. T. Elliott and K. Campbell, Current trends in rapid tests for mycotoxins, *Food Addit. Contam.,:Part A*, 2019, **36**, 800–814.
5 C. Chartrand, M. M. Leeflang, J. Minion, T. Brewer and M. Pai, Accuracy of rapid influenza diagnostic tests: a meta-analysis, *Ann. Intern. Med.*, 2012, **156**(7), 500–511.
6 F. Li, M. You, S. Li, J. Hu, C. Liu and Y. Gong, *et al.*, Paper-based point-of-care immunoassays: Recent advances and emerging trends, *Biotechnol. Adv.*, 2020, **39**, 39–107442.
7 T. Mahmoudi, M. de la Guardia, B. Shirdel, A. Mokhtarzadeh and B. Baradaran, Recent advancements in structural improvements of lateral flow assays towards point-of-care testing, *TrAC, Trends Anal. Chem.*, 2019, **116**, 13–30.
8 Y. Liu, L. Zhan, Z. Qin, J. Sackrison and J. C. Bischof, *Ultrasensitive and Highly Specific Lateral Flow Assays for Point-of-Care Diagnosis*, ACS Nano, 2021, vol. 15, pp. 3593–3611.
9 P. Peng, C. Liu, Z. Li, Z. Xue, P. Mao and J. Hu, *et al.*, Emerging ELISA derived technologies for in vitro diagnostics, *TrAC, Trends Anal. Chem.*, 2022, **152**, 116605.
10 K. Wu, X. He, J. Wang, T. Pan, R. He and F. Kong, *et al.*, Recent progress of microfluidic chips in immunoassay, *Front. Bioeng. Biotechnol.*, 2022, **10**, 1112327.
11 W. Alahmad, A. Sahragard and P. Varanusupakul, Online and offline preconcentration techniques on paper-based analytical devices for ultrasensitive chemical and biochemical analysis: A review, *Biosens. Bioelectron.*, 2021, **194**, 113574.
12 S. Augustine, M. V. Chinnamani, C. W. Mun, J. Y. Shin, T. Q. Trung and S. J. Hong, *et al.*, Metal-enhanced fluorescence biosensor integrated in capillary flow-driven microfluidic cartridge for highly sensitive immunoassays, *Biosens. Bioelectron.*, 2024, **248**, 115987.
13 C. P. Jia, X. Q. Zhong, B. Hua, M. Y. Liu, F. X. Jing and X. H. Lou, *et al.*, Nano-ELISA for highly sensitive protein detection, *Biosens. Bioelectron.*, 2009, **24**(9), 2836–2841.
14 Z. Qu, H. Xu, P. Xu, K. Chen, R. Mu and J. Fu, *et al.*, Ultrasensitive ELISA using enzyme-loaded nanospherical brushes as labels, *Anal. Chem.*, 2014, **86**(19), 9367–9371.
15 H. Jie, Y. Wang, M. Zhao, X. Wang, Z. Wang and L. Zeng, *et al.*, Automatic ultrasensitive lateral flow immunoassay based on a color-enhanced signal amplification strategy, *Biosens. Bioelectron.*, 2024, **256**, 116262.
16 P. Nandhakumar, C. Muñoz San Martín, B. Arévalo, S. Ding, M. Lunker and E. Vargas, *et al.*, Redox Cycling Amplified Electrochemical Lateral-Flow Immunoassay: Toward Decentralized Sensitive Insulin Detection, *ACS Sens.*, 2023, **8**(10), 3892–3901.
17 Y. Song, J. Zhao, T. Cai, A. Stephens, S. H. Su and E. Sandford, *et al.*, Machine learning-based cytokine microarray digital immunoassay analysis, *Biosens. Bioelectron.*, 2021, **180**, 113088.
18 B. Y. Moghadam, K. T. Connelly and J. D. Posner, Two orders of magnitude improvement in detection limit of

lateral flow assays using isotachophoresis, *Anal. Chem.*, 2015, **87**(2), 1009–1017.

19 S. Park, K. Buhnik-Rosenblau, R. Abu-Rjal, Y. Kashi and G. Yossifon, Periodic concentration-polarization-based formation of a biomolecule preconcentrate for enhanced biosensing, *Nanoscale*, 2020, **12**(46), 23586–23595.

20 S. Osman, E. L. Claus and R. K. Anand, Label-Free, Non-Optical Readout of Bead-Based Immunoassays with and without Electrokinetic Preconcentration, *Anal. Chem.*, 2023, **95**(24), 9337–9346.

21 A. Sharma, A. I. Y. Tok, C. Lee, R. Ganapathy, P. Alagappan and B. Liedberg, Magnetic field assisted preconcentration of biomolecules for lateral flow assaying, *Sens. Actuators, B*, 2019, **285**, 431–437.

22 J. R. Wiśniewski, A. Zougman, N. Nagaraj and M. Mann, Universal sample preparation method for proteome analysis, *Nat. Methods*, 2009, **6**(5), 359–362.

23 E. Fornells, E. F. Hilder and M. C. Breadmore, Preconcentration by solvent removal: techniques and applications, *Analytical and Bioanalytical Chemistry*, Springer Verlag, 2019, vol. 411, pp. 1715–1727.

24 D. Ross and L. E. Locascio, Microfluidic temperature gradient focusing, *Anal. Chem.*, 2002, **74**(11), 2556–2564.

25 C. Kim, Y. K. Yoo, N. E. Lee, J. Lee, K. H. Kim and S. Lee, *et al.*, Nanoelectrokinetic-assisted lateral flow assay for COVID-19 antibody test, *Biosens. Bioelectron.*, 2022, **212**, 114385.

26 J. Choi, S. Baek, H. C. Kim, J. H. Chae, Y. Koh and S. W. Seo, *et al.*, Nanoelectrokinetic Selective Preconcentration Based on Ion Concentration Polarization, *BioChip J.*, 2020, **14**, 100–109.

27 Y. C. Wang, A. L. Stevens and J. Han, Million-fold preconcentration of proteins and peptides by nanofluidic filter, *Anal. Chem.*, 2005, **77**(14), 4293–4299.

28 B. Sabbagh, S. Park and G. Yossifon, Microvalve-Based Tunability of Electrically Driven Ion Transport through a Microfluidic System with an Ion-Exchange Membrane, *Anal. Chem.*, 2023, **95**(16), 6514–6522.

29 S. J. Kim, Y. A. Song and J. Han, Nanofluidic concentration devices for biomolecules utilizing ion concentration polarization: Theory, fabrication, and applications, *Chem. Soc. Rev.*, 2010, **39**(3), 912–922.

30 A. Krishnamurthy and R. K. Anand, Recent advances in microscale extraction driven by ion concentration polarization, *TrAC, Trends Anal. Chem.*, 2022, **148**, 116537.

31 K. Kim, W. Kim, H. Lee and S. J. Kim, Stabilization of ion concentration polarization layer using micro fin structure for high-throughput applications, *Nanoscale*, 2017, **9**(10), 3466–3475.

32 B. Berzina, U. Peramune, S. Kim, K. Saurabh, E. L. Claus and M. E. Strait, *et al.*, Electrokinetic Enrichment and Label-Free Electrochemical Detection of Nucleic Acids by Conduction of Ions along the Surface of Bioconjugated Beads, *ACS Sens.*, 2023, **8**(3), 1173–1182.

33 B. Berzina and R. K. Anand, An Electrokinetic Separation Route to Source Dialysate from Excess Fluid in Blood, *Anal. Chem.*, 2018, **90**(6), 3720–3726.

34 W. Ouyang and J. Han, Universal amplification-free molecular diagnostics by billion-fold hierarchical nanofluidic concentration, *Proc. Natl. Acad. Sci. U. S. A.*, 2019, **116**(33), 16240–16249.

35 J. Choi, K. Huh, D. J. Moon, H. Lee, S. Y. Son and K. Kim, *et al.*, Selective preconcentration and online collection of charged molecules using ion concentration polarization, *RSC Adv.*, 2015, **5**(81), 66178–66184.

36 S. Lee, S. Park, W. Kim, S. Moon, H. Y. Kim and H. Lee, *et al.*, Nanoelectrokinetic bufferchannel-less radial preconcentrator and online extractor by tunable ion depletion layer, *Biomicrofluidics*, 2019, **13**(3), 034113.

37 Y. Green, S. Shloush and G. Yossifon, Effect of geometry on concentration polarization in realistic heterogeneous permselective systems, *Phys. Rev. E: Stat., Nonlinear, Soft Matter Phys.*, 2014, **89**(4), 043015.

38 T. A. Zangle, A. Mani and J. G. Santiago, On the propagation of concentration polarization from microchannel - nanochannel interfaces Part II: Numerical and experimental study, *Langmuir*, 2009, **25**(6), 3909–3916.

39 D. Malamud and J. W. Drysdale, Isoelectric Points of Proteins: A Table, *Anal. Biochem.*, 1978, **86**, 620–647.

40 G. Yossifon and H. C. Chang, Changing nanoslot ion flux with a dynamic nanocolloid ion-selective filter: Secondary overlimiting currents due to nanocolloid-nanoslot interaction, *Phys. Rev. E: Stat., Nonlinear, Soft Matter Phys.*, 2010, **81**(6), 066317.

41 W. Kusnezow, Y. V. Syagailo, S. Rüffer, K. Klenin, W. Sebald and J. D. Hoheisel, *et al.*, Kinetics of antigen binding to antibody microspots: Strong limitation by mass transport to the surface, *Proteomics*, 2006, **6**(3), 794–803.

42 W. Kusnezow, Y. V. Syagailo, I. Goychuk, J. D. Hoheisel and D. G. Wild, Antibody micoarrays: The crucial impact of mass transport on assay kinetics and sensitivity, *Expert Rev. Mol. Diagn.*, 2006, **6**, 111–124.

43 E. P. Brown, A. F. Licht, A. S. Dugast, I. Choi, C. Bailey-Kellogg and G. Alter, *et al.*, High-throughput, multiplexed IgG subclassing of antigen-specific antibodies from clinical samples, *J. Immunol. Methods*, 2012, **386**(1–2), 117–123.

44 S. Lin, A. Shih-Yuan Lee, C. C. Lin and C. K. Lee, Determination of Binding Constant and Stoichiometry for Antibody-Antigen Interaction with Surface Plasmon Resonance, *Curr. Proteomics*, 2006, **3**, 271–282.